Quantifying the quality of optical vortices by evaluating their intensity distributions

Mateusz Szatkowski (mateusz.szatkowski@pwr.edu.pl)
Wrocław University of Science and Technology
Brandon Norton
University of North Carolina at Charlotte
Jan Masajada
Wrocław University of Science and Technology
Rosario Porras-Aguilar
University of North Carolina at Charlotte

Research Article

Keywords:

Posted Date: December 10th, 2021

DOI: https://doi.org/10.21203/rs.3.rs-1156292/v1

Quantifying the quality of optical vortices by evaluating their intensity distributions

Mateusz Szatkowski[1,2,*], Brandon Norton[2], Jan Masajada[1], Rosario Porras-Aguilar[2]

[1]Wrocław University of Science and Technology, Wrocław, 50-370, Poland.
[2]University of North Carolina at Charlotte, Charlotte, North Carolina, 28223, USA.
[*]mateusz.szatkowski@pwr.edu.pl

Abstract

Optical vortices are widely used in optics and photonics, ranging from microscopy and communications to astronomy. However, little work has been done to quantify the quality of scalar optical vortices. Since the quality of an optical vortex affects measurements and conclusions derived from their use, it is crucial to develop tools to evaluate it efficiently. Moreover, the quality of a vortex strongly depends on the application. Therefore, this work aims to establish metrics for the evaluation of optical vortex quality. We propose to evaluate vortex quality using the following intensity parameters: eccentricity of the intensity distribution, cross-sectional peak-to-valley measurements, cross-sectional peak difference, and the ratio of the ring width to the vortex core diameter (doughnut-ratio). These parameters can be used as a guide for the quality of optical vortices depending on their implementation for specific optical technologies.

Introduction

Optical vortices are widely used in optics and photonics, ranging from superresolution microscopy[1–3], through optical manipulation[4,5], enlarging the bandwidth in optical communications[6–8], to the discovery of exoplanets in astronomy[9–11]. Still, not enough work has been done to evaluate the quality of the scalar optical vortex itself. Furthermore, the definition of "a good optical vortex" differs depending on the specific application.

Optical vortices are stable phase singularities with a spiral wavefront. The optical field's phase singularity brings peculiar vortex features, such as zero intensity point at the center of the beam (vortex core), responsible for a characteristic doughnut-like intensity distribution. A beam with an embedded optical vortex carries an orbital angular momentum (OAM), defined as $l\hbar$ per photon, where l denotes the topological charge – the number of wavefront twists around the optical axis.

Optical vortices are a natural phenomenon existing across various optical fields, with a speckle field full of randomly generated optical vortices, as the best example. Due to increasing interest in light structuring, multiple methods to generate optical vortices have been proposed over the years. Two of the most popular methods are based on either refractive elements or various types of liquid crystals on silicon spatial light modulators (SLMs)[12]. These two directly introduce the spiral phase profile into the upcoming beam, transforming it into an optical vortex.

The quality of the optical vortex will affect the implementation of each optical technology in a different fashion. For instance, in optical trapping, for whom Artur Ashkin[13] was awarded the Noble Prize in 2018, the vortex beam will transfer its OAM to the trapped particle. This will result in particle rotation around the optical axis; thus, the quality of the optical vortex will primarily impact the trajectory of this rotation. Therefore, the vortex quality can be evaluated through the rotation dynamics[14]. On the other hand, stimulated emission depletion (STED) microscopy, Noble Prize in 2014 for superresolution, will define the

quality of the vortex in terms of its potential to provide depletion and precision of such process. In this case, the requirements are the vortex beam diameter, vortex contrast, and its symmetry[15]. Optical metrology based on the use of vortices as a scanning tool will rely on the tracking accuracy of the vortex core (intensity dark point and its close vicinity)[16]. Another example is in optical communication systems that evaluate the modal dispersion[17] or vortex capability to sustain atmospheric turbulence when considering the free-space propagation[18]. Finally, in exoplanet detection, telescopes that incorporate vortices or vector vortex beams to dim the starlight require various parameters to characterize the overall performance of vortex coronagraphy[19].

All of these areas depend on beam shaping, referring to the control of light's parameters such as amplitude, phase, and polarization. Therefore, developing light structuring and evaluating tools as a part of fundamental research devoted to beam shaping is crucial for each of mentioned applications. More specifically, the quality of the optical vortex can influence any measurement and conclusions derived from multiple applications where vortices are implemented. This manuscript was motivated by the relevance of using optical vortices in modern optical technology and the lack of sense of what is considered a relatively good optical vortex.

Therefore, this work aims to establish guidelines to evaluate the quality of an optical vortex. We propose a simple tool to quantify the vortex quality based on selected parameters calculated out of the vortex intensity image. These indicators describe the quality of the optical vortex and suggest what can be done to improve the vortex condition.

We underline that this work does not aim to correct the vortex beam. This issue has been studied in various research papers over the years[20,21]. Instead, we would like to focus on how far one should go experimentally to improve the vortex itself.

Methods

Figure 1a-d shows four examples of the optical vortex intensity distribution in the experimental setup presented in Figure 1e. The experimental parameters that led to each vortex image were slightly modified. Thus, even though the images clearly show deformations or intensity saturation, they can still be considered high-quality optical vortices, depending on the application.

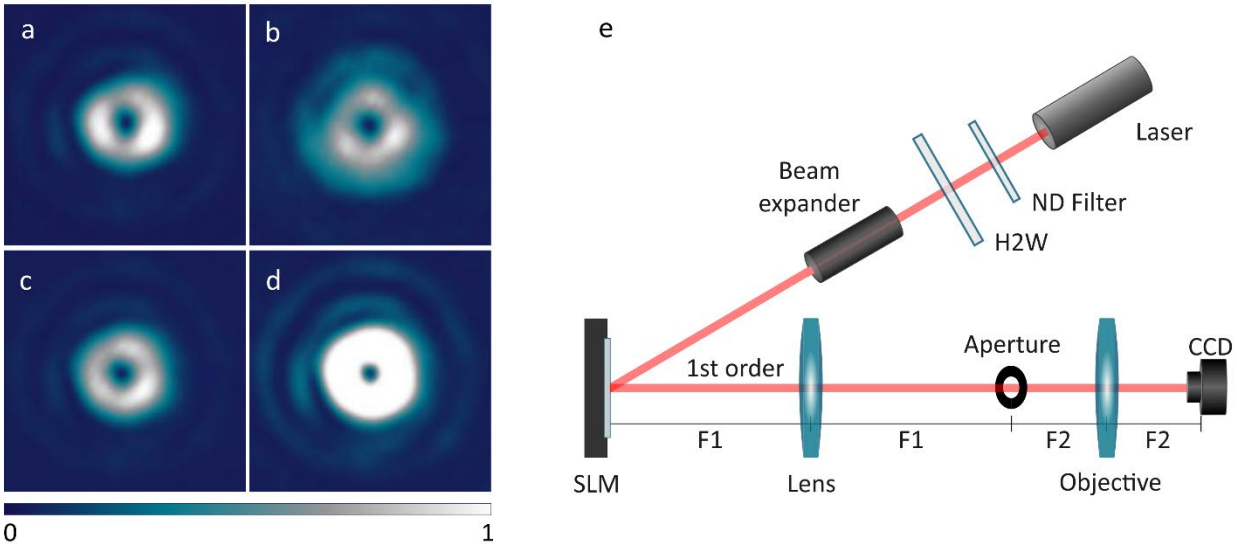

Figure 1. a) – d) Different intensity distributions of an optical vortex of topological charge $l = 1$, generated by the SLM e) The general scheme of the experimental system

The following sections will represent the scenarios shown in Figure 1a in terms of four parameters: eccentricity, peak-to-valley, peak difference, and doughnut-ratio to evaluate the quality of the optical vortex. Each parameter is linked with a specific practical example, where it can be directly applied and discuss how the modification of the experimental setup and artifacts impact particular parameters.

Eccentricity

Eccentricity in an optical vortex refers to the vortex symmetry in the intensity distribution. Interestingly, the eccentricity parameter depends on experimental conditions as the resolution used to sample the spiral phase distribution and astigmatism introduced in the optical system. Therefore, let us start the analysis by deriving an equation that describes eccentricity.

The a priori knowledge about the existence of the vortex inside the beam leads to a simple relation between the detected intensity signal $I(x,y)$ and its pseudo-complex analytic signal $\tilde{I}(x,y)$, given by

$$\tilde{I}(x,y) = I(x,y) * \mathbf{LG}(x,y), \tag{1}$$

where, $\mathbf{LG}(x,y)$ denotes the Laguerre-Gaussian filter, described as

$$\mathbf{LG}(x,y) = F^{-1}\{LG(f_x,f_y)\} = (j\pi^2\omega^4)(x+jy)exp(-\pi^2\omega^2(x^2+y^2)) = (j\pi^2\omega^4)(r\ exp(-\pi^2r^2\omega^2)exp(j\alpha)). \tag{2}$$

Here, F^{-1} denotes the inverse Fourier transform, the terms $r = \sqrt{x^2+y^2}$ and $\alpha = arctan(x/y)$, express the spatial polar coordinates. The bandwidth ω is the variable parameter, which should match the size of the vortex core. The function $LG(f_x,f_y)$ describes the Laguerre-Gaussian filter in the Fourier domain and is described as follows,

$$LG(f_x,f_y) = \rho\ exp(-\rho^2/\omega^2)\exp(j\beta), \tag{3}$$

with $\rho = sqrt(x^2+y^2)$, $\beta = \arctan(f_x/f_y)$ both representing the polar coordinates.

It is important to note that $\tilde{I}(x,y)$ in Eq. (1), describes the pseudo-complex amplitude since the pseudo-phase represented in $\mathbf{LG}(x,y)$ is not real. However, it can still provide valuable information about the measured signal. Following the equation (1), the real and imaginary part in the close vicinity of the vortex core can be approximated as,

$$Re[\tilde{I}(x,y)] = a_r x + b_r y + c_r, \qquad Im[\tilde{I}(x,y)] = a_i x + b_i y + c_i, \tag{4}$$

where the coefficients a_k, b_k, and c_k are provided by linear polynomial surface approximation of real $k = r$ and imaginary $k = i$ parts, respectively.

From equations (4), it is possible to calculate the eccentricity as follows[22],

$$e = \sqrt{1 - \frac{\left(a_r^2 + a_i^2 + b_r^2 + b_i^2\right) - \sqrt{\left(a_r^2 + a_i^2 - b_r^2 - b_i^2\right)^2 + 4(a_r b_r + a_i b_i)^2}}{\left(a_r^2 + a_i^2 + b_r^2 + b_i^2\right) + \sqrt{\left(a_r^2 + a_i^2 - b_r^2 - b_i^2\right)^2 + 4(a_r b_r + a_i b_i)^2}}}. \tag{5}$$

Here $e = 0$ denotes the perfect circle and $e \in (0, 1)$ represents an ellipse.

The eccentricity is given in Eq. (5) becomes a valuable parameter to describe the general shape of the optical vortex serving as a description of the vortex symmetry, no matter the reason of vortex distortion. The range of applications of this parameter is practically unlimited. It can range from evaluation of atmospheric turbulence through optical trapping and aberrometry. To further examine the concept of eccentricity in optical vortices, we evaluated the behavior of eccentricity as a function of the phase steps to reconstruct the spiral and alignment errors.

The impact of reduced phase resolution, defined as the phase increment along the spiral phase gradient of vortex generating element, has been studied before in the context of spiral phase plates – refractive vortex generating elements[23,24]. However, we incorporated the eccentricity to a similar analysis and evaluated the quality of the vortex beam under the impact of the reduced phase resolution. We studied the eccentricity evolution for a phase gradient ranging from 3 to 255 steps across the [0, 2π] phase range. Figure 2 presents exemplary results, with both phase and intensity profile of the obtained beam, together with the intensity contour plot that visualizes the vortex core geometry. The eccentricity values predicted in Figure 2c are the most symmetric ($e = 0.09$), visually Figure 2b and c are very similar. The inserted images show both the phase and intensity distribution of the subsequent optical vortices.

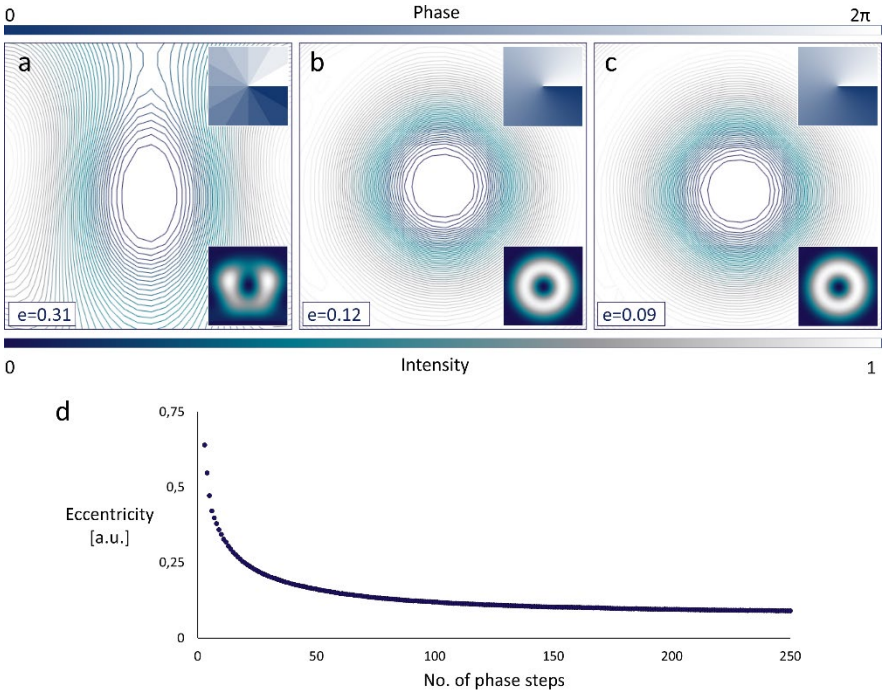

Figure 2. The figure presents the intensity contour plot of three separate optical vortices simulated numerically, where the spiral phase responsible for the generation of the optical vortex is divided into a) 12, b) 100, c) 255 steps across the [0, 2π] phase range. The eccentricity value given by the Laguerre-Gaussian transform is equal to a) 0.31 b) 0.18 and c) 0.09, respectively

Figure 2d. shows a more detailed behavior of the eccentricity under the impact of the reduced phase resolution on the eccentricity of the vortex core. The eccentricity is calculated for any number of phase steps used to generate an optical vortex ranging from 3 to 255. The increase in the number of phase steps improves the vortex symmetry, which reaches $e = 0.09$ for the 255 phase steps which corresponds to 255 grayscale values. The results show that increased phase resolution has a remarkable impact on the vortex

symmetry. This is not a problem for vortices generated using SLMs with 255 grayscale values or more. However, eccentricity also serves as a direct result to assist the user with the setup alignment.

One of the most typical alignment errors is astigmatism caused by the tilt of optical components. This astigmatism destroys the vortex beam in a distinctive way, strongly influencing the shape of the vortex core[25,26]. We analyzed the impact of astigmatism both numerically and experimentally on the eccentricity value (Figure 3). Astigmatism, defined by Zernike polynomial Z_2^{-2}, has been introduced artificially through the modification of the vortex hologram displayed by the SLM. The lack of aberration $Z_2^{-2} = 0$ corresponded to the lowest eccentricity $e = 0.09$. The eccentricity increased dramatically together with the increase of astigmatism and reached $e = 0.94$ for astigmatism $Z_2^{-2} = \lambda$ and $Z_2^{-2} = -\lambda$ defined over the optical system aperture, as shown in Figure 3.

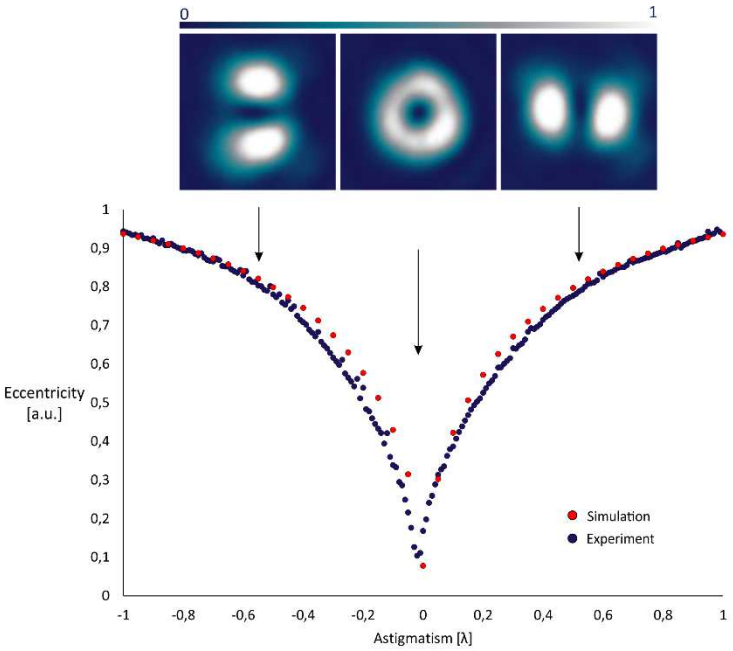

Figure 3. The eccentricity evolution due to introduced astigmatism. Astigmatism is defined by the Z_2^{-2} Zernike polynomial, across the optical system aperture. The top part of the figure presents three experimental vortex intensity distributions. The central refers to the vortex without aberration. The bottom part of the figure shows both numerical (red) and experimental (blue) data.

As discussed so far, the eccentricity provides a fast measurement of vortex quality. Unfortunately, it is impossible to connect it with the direct source of vortex distortion. In other words, the same eccentricity value can be calculated for two opposite values of astigmatism, as shown in Figure 3. Therefore, it does not provide any specific directions on how the user can improve the vortex quality. The following paragraphs propose additional parameters to support the eccentricity in determining the vortex beam quality.

Peak-to-valley

The first parameter will refer to one of the essential features of an optical vortex, a singular point that emerged as zero intensity point in the beam. In this context, the peak-to-valley $\overline{PV}$ is defined as the mean intensity difference between the maximum and minimum value across *x* and *y* beam intensity profiles:

$$\overline{PV} = 0.5 \sum_{i=1}^{2} PV_i \tag{6}$$

where PV_i stands for the peak-to-valley across two perpendicular intensity profiles, defined as:

$$PV_i = max(I_1, I_2) - I_{min}. \tag{7}$$

I_1, I_2 are the values of two maxima across the *x*- and *y*-axis of the vortex intensity profile, respectively, and I_{min} defines the value of minimum intensity located at the vortex core. The peak-to-valley for the perfect optical vortex should be equal to 1, followed by the intensity profile symmetry so that $I_1 = I_2$. In the real experimental environment, this is never achieved, and minor differences between I_1 and I_2 are expected as long as the beam is not saturated. Our algorithm first defines two maxima I_1 and I_2, then selects the one that has the higher value and uses that to evaluate the peak-to-valley parameter. Therefore, even if these two peaks are highly asymmetrical, this parameter aims not to evaluate the symmetry of the beam but to define the contrast of the vortex image. To assure that the various aspects of the image are considered, the algorithm takes the mean peak-to-valley value across two perpendicular profiles along the *x*- and *y*-axis.

In typical setups, this is a valuable factor to determine the correct camera settings by evaluating the impact of the background light on the optical vortex intensity range. Whenever the additional background illumination persists, it increases the amount of light visible in the vortex dark spot, leading to the reduced peak-to-valley ratio. This relation is visually presented in Figure 4, where illumination in plot a) is 0, while plot b) shows an offset due to background illumination.

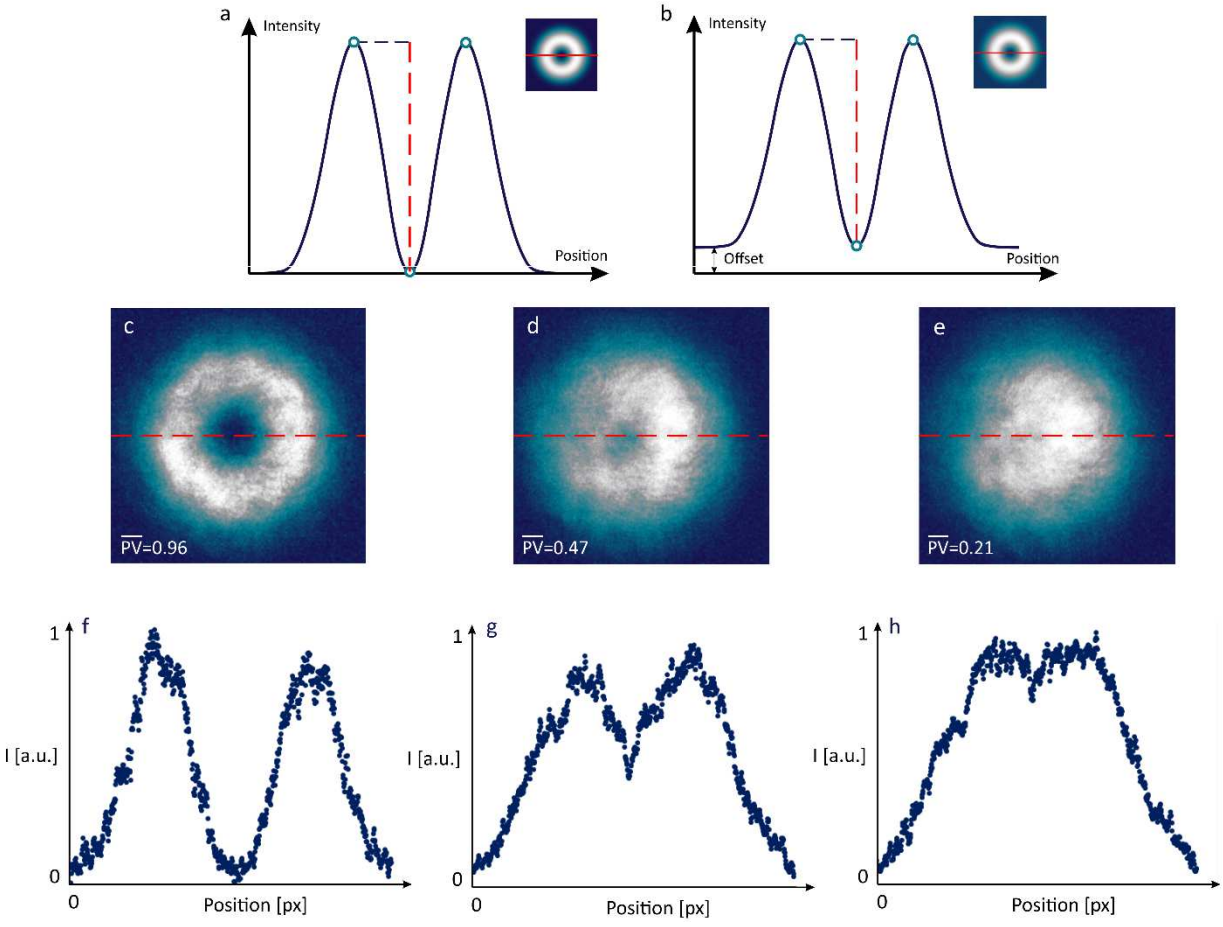

Figure 4. Schematic representation of the peak-to-valley parameter, marked by the dashed red line. Optical vortex intensity profiles of a) ideal optical vortex and b) optical vortex with additional background illumination. The intensity distributions of each vortex are inserted in the subfigures. The intensity profile was taken along the solid red line, visible in the inserted distributions. c) to e)

Experimental images of a partially coherent optical vortex. The degree of coherence reduces from c) to e), and the calculated $\overline{PV}$ value is inserted in each image. f) to h) Intensity profiles taken across dashed lines inserted in the intensities images above, respectively. Experimental data courtesy of Benjamin Perez Garcia from Tecnologico de Monterrey.

Nevertheless, the background light is not the only factor that may affect the intensity of a singular point. Such a point is a peculiar feature of each optical vortex, being a pure interference phenomenon. Therefore, it directly follows all of the requirements for interference, such as spatial and temporal coherence[27,28]. Thus, the peak-to-valley value can be directly linked with the vortex degree of coherence. Any lack of coherence does not lead to a loss in vortex symmetry but directly reduces the peak-to-valley ratio, as shown in Figure 4c-h.

The singular point slowly vanishes, and the beam resembles the Gaussian laser mode, which is reached after the peak-to-valley is reduced to 0. Peak-to-valley serves as a fast and efficient way to examine the coherence of vortex beam, being a relevant quality factor, wherever the low coherent source of light is applied. Apart from this fundamental research on singular optics, the range of applications where $\overline{PV}$ can be directly incorporated involves astronomy, particularly vortex coronagraphy, where vortex generating elements aim to reduce the bright start light by introducing an optical vortex. $\overline{PV}$ together with other parameters proposed in this work can be an efficient way to evaluate the vortex quality, impacting the performance of the vortex coronagraph in the actual experimental tasks.

Peak difference

The intensity within the singular point is not the only issue that may affect the quality of an optical vortex. One of the main challenges of aligning the optical setup is positioning an optical vortex within the laser beam. The off-axis optical vortex can be appropriate for particular applications such as vortex scanning microscopy[29], where the vortex core is used as an object scanner. In most applications, a symmetric, centered optical vortex is more desired. Fortunately, any misalignment emerges itself as a disproportion of the intensity peak values, which can be evaluated through the *peak difference* parameter defined as,

$$\overline{PD} = 0.5 \sum_{i=1}^{2} PD_i, \tag{8}$$

where PD_i defines the peak difference across two perpendicular intensity profiles (x and y), each representing the absolute difference between two intensity peaks across a particular intensity profile,

$$PD_i = |I_1 - I_2|. \tag{9}$$

Figure 5a-b shows the peak difference parameter for a simulated intensity distribution of an off-axis vortex. The $\overline{PD} = 0$, for a perfectly symmetric optical vortex; however, this is impossible to achieve in the experimental environment unless the image is saturated. The peak difference value will be larger as the optical vortex is positioned further away from the optical axis. As expected, the movement of the vortex at the image plane is perpendicular to the direction of the vortex shift at the object plane.

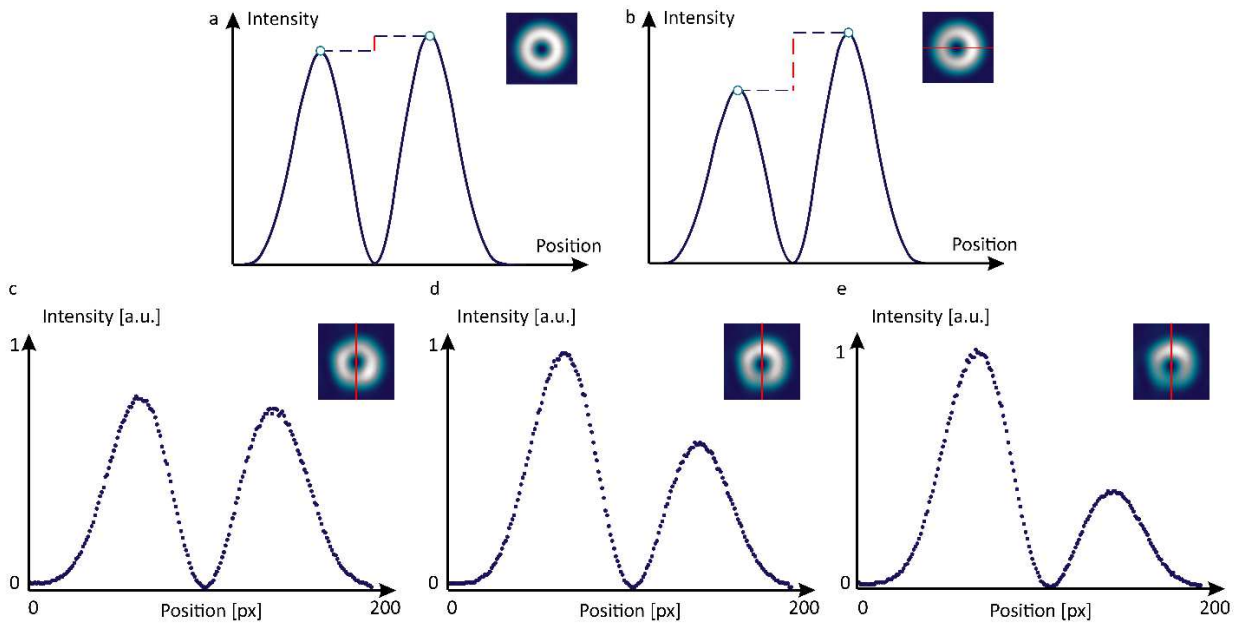

Figure 5. Schematic representation of the peaks difference parameter, marked by the dashed red line. Optical vortex intensity profiles of a) an optical vortex shifted by 16 microns at the object plane and b) 80 microns shifted at the object plane. The intensity distributions of the particular optical vortex are inserted in the subfigures. The intensity profile was taken along the *x*-axis, marked by the solid red line, visible in the inserted distributions. c)-e) Experimental beam intensity profiles, taken for the optical vortex when it is c) experimentally close to the center with PD =0.06, d) shifted by 24 pixels at the SLM with PD =0.37, and e) shifted 112 pixels at the SLM with PD=0.55. The intensity distributions of the particular optical vortex are inserted in the subfigures. The intensity profile was taken along the y axis, marked by the solid red line, visible in the inserted distributions.

Similarly, we calculated the peak difference parameter for experimental images of an optical vortex when shifted off-axis. Figure 5c-e shows the intensity distributions of an optical vortex that was shifted horizontally[30,31].

Some differences in the maximum intensity on each plot are visible, which is an expected result since the intensity was not normalized at any point. This, however, has no impact on the calculation of the peak difference parameter. As visible in Figure 5c-e, images were not saturated, leaving room for longer camera exposure time or increased total laser power. Our algorithm measures the PD along the *x* and *y*-axis to assist the user in realigning the optical vortex. In practice, the primary source of decentralization is related to the non-uniform illumination of the vortex-generated element. Therefore, the vortex positioning in reference to the laser beam is crucial wherever the vortex has to be separately introduced through the external beam shaping. It should not be an issue for vortices generated directly inside the laser cavity[32,33]. However, it becomes more critical in vortex generation methods that use refractive elements or spatial light modulators. This issue emerges in any application that relies on proper vortex intensity distribution. The obvious example of such is STED microscopy, where the lack of symmetry will impact the quality of depletion. Any disproportions that arise from the decentralization of vortex generating element in reference to the beam lead to an increase of the peak difference, directly impacting the depletion and allowing the fluorescence to occur in the unwanted parts of the sample.

Doughnut-ratio

No less important than the vortex symmetry is an appropriate doughnut shape, the typical feature of the Laguerre-Gaussian mode. Whenever the spiral phase profile is introduced to the Gaussian beam, the optical vortex is created and evolves with the propagation distance to obey the paraxial wave equation. Thus, it

slowly resembles a Laguerre-Gaussian mode, which is reached in the far-field. The phase-amplitude modulation can directly shape the light into Laguerre-Gaussian mode so that far-field propagation is not needed. Another way is to focus the beam, where the optical system creates the real image of the "closed" optical vortex. Often this is neglected, showing an optical vortex without the proper doughnut shape. One approach to this issue is to calculate the correlation between the experimentally generated optical vortex and its ideal simulation[34]. However, it requires additional computational effort and relies on the appropriate and accurate size of the simulated vortex, which depends on the chosen aperture. We propose a less demanding approach that can directly evaluate the vortex intensity distribution and doughnut shape from a single intensity image. This parameter is based on the ratio of the dark hollow diameter in relation to the bright ring's width, at half of the maximum beam intensity,

$$\bar{R} = 0.5 \sum_{i=1}^{2} R_i, \tag{10}$$

where R_i defines the doughnut-ratio across two perpendicular intensity profiles, typically x and y, each represents the mean *ratio* between the diameter of the vortex core and the width of the bright ring on the left and the right side, both defined at $0.5\ I_{max}$ level,

$$R_i = 0.5 \cdot \left[\frac{|P_2 - P_1|}{|P_3 - P_2|} + \frac{|P_4 - P_2|}{|P_3 - P_2|} \right]. \tag{11}$$

The visual example is schematically shown in Figure 6a, where the cross-section of the intensity profile with the $0.5\ I_{max}$ line is shown. Here, the distances between P_1 and P_2, together with P_3 and P_4 denote the ring's width, while the distance between P_2 and P_3 denotes the vortex core diameter.

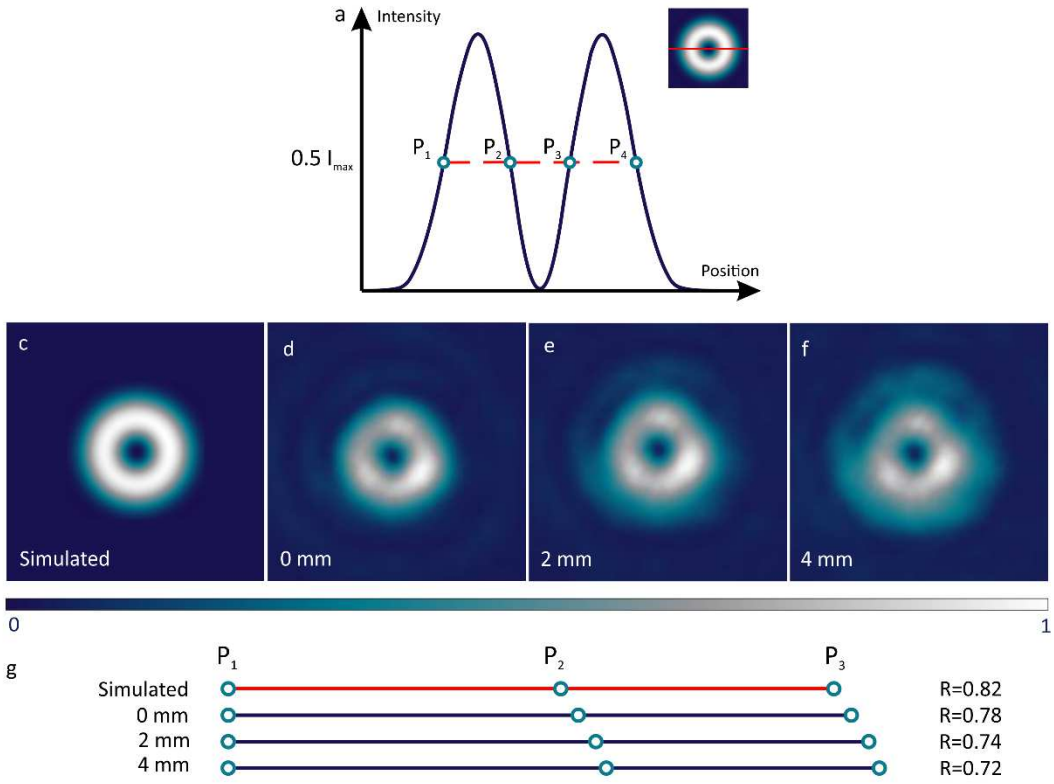

Figure 6. Schematic representation of the ratio parameter. The intensity profile of the ideal optical vortex is presented, together with the red dashed line, marking the position of the 0.5 I_max level. The crosssection of this line with the intensity profile is marked by circles. c) Numerically simulated image of an optical vortex, R=0.82. d) Experimental image of an optical vortex at the focal plane, R=0.78, e) 2 mm behind the focal plane, R=0.74, and f) 4 mm behind the focal plane, R=0.72, respectively. g) Evolution of the bright ring's width and the vortex core diameter for each of the above cases. Points are analogical to those depicted in a).

Based on this definition, the ratio parameter is equal to 0.82 for an ideal Laguerre-Gaussian beam. This value does not change with propagation, and it is also independent of the Gaussian beam's waist[35]. Therefore, we can use this parameter to compare numerical with experimental data at different observation planes (at 0, 2, and 4 mm, respectively). These results are presented in Figure 6c-f. The beam expanded with the shift of the observation plane, simultaneously changing the $\bar{R}$, which started to decrease with the observation plane.

The doughnut-ratio parameter can evaluate an independent feature of the optical vortex, e.g., the shape of the intensity envelope. While various factors can affect the $\bar{R}$ deviation from the ideal case, we differentiate a few, the most important in laser beam shaping. The lack of focal plane and already explained importance of the focal plane position for vortex quality[34]. The role of ratio can go far beyond beam shaping and can be applied to the automatization of an optical setup that requires an optical vortex, at least just as a focal plane marker. The parameter $\bar{R}$ can also be used to determine if the image is saturated or not. For a saturated image, $\bar{R}$ will be largely reduced due to the widening of the vortex doughnut. Last but not least, it can evaluate the chosen numerical aperture. If the aperture becomes too small, the diffracted beam will not lead to the proper ratio, the one resembling an ideal Laguerre-Gaussian mode.

Discussion and Conclusions

In this manuscript, we propose the use of four parameters to evaluate the quality of an optical vortex, eccentricity, peak-to-valley, peak difference, and doughnut-ratio. Table 1 summarizes the experimental

conditions resulting from the vortex quality change and the optical technologies where this parameter is crucial. The parameters complement each other to provide crucial information to evaluate the vortex quality.

Table 1. Table links the proposed parameters with their experimental features. Further, it suggests the relevant optical fields that may benefit by applying a particular parameter.

Parameter	**Vortex Evaluation**	**Optical field relevance**
Eccentricity	General vortex symmetry	Optical communication, aberrometry
Peak-to-valley	Background light, camera resolution, and coherence	Fundamental research on partially coherent optical vortices, Optical setup alignment
Peak difference	Vortex position (off-axis shift), non-central beam illumination, camera saturation	Optical metrology, STED or vortex scanning microscopy
Doughnut-ratio	Focal plane, camera saturation, diffraction, vortex core diameter	Research on the optical vortex propagation, Optical setup alignment,

Following the methodology proposed in this manuscript, we have developed a script that can be used to analyze vortices in the experimental practice. As an example, we have analyzed each of the vortices shown in Figure 1. Table 2. provides the values of each of the four parameters proposed in this work.

Table 2. Optical vortex quality quantification by the introduced parameters. Evaluated vortices are presented in Figure 1, and the same subfigure indicators are used.

Subfigure of Figure 1	**Eccentricity**	**PV**	**PD**	**R**
a	0.12	0.75	0.02	0.62
b	0.16	0.96	0.10	0.67
c	0.12	0.95	0.06	0.76
d	0.15	0.84	0	0.30

Vortices in Figure 1a) and c) are the most symmetric due to the lowest eccentricity, but b) and d) are not much worse. Case a) has a relatively low PV, which may suggest low coherence, but considering $\bar{R}$, it does not resemble an ideal Laguerre – Gaussian mode but more likely has astigmatism within the beam. Vortex in Figure 1b) shares the $\bar{R}$ value with a), but the $\overline{PD}$ indicates that it may be slightly off-axis. Vortex in d) is not only to some extent asymmetric (eccentricity), but also highly saturated, giving 0 in $\overline{PD}$ (unachievable experimentally for a non-saturated beam). Due to this saturation, it also has the lowest $\bar{R}$ among all examples. Vortex c) leads in most of these parameters and could be considered the best among all given examples. Nevertheless, the $\bar{R}$ parameter can be improved, which implies that the vortex was slightly out of focus.

In conclusion, the methodology proposed here can be used as a guide to determine the optical vortex's qualities depending on the specific optical technology. This work examines vortices in various ways, leading to multiple quality criteria, each sensitive to a different aspect of the implementation and optical setup alignment. The method is easy to implement in any optical system, as long as the intensity image is obtained. It is versatile and not associated with any particular method of optical vortex generation. The script of the vortex evaluation is available in the open-access repository[36]. We would like to underline that it is the user who eventually evaluates the vortex beam. This tool aims to provide assistance, making the final decision more practical.

References

1. Gbur, G. Using superoscillations for superresolved imaging and subwavelength focusing. *Nanophotonics* **8**, 205–225 (2018).
2. Popiołek-Masajada, A., Masajada, J. & Szatkowski, M. Internal scanning method as unique imaging method of optical vortex scanning microscope. *Optics and Lasers in Engineering* **105**, 201–208 (2018).
3. Willig, K. I., Harke, B., Medda, R. & Hell, S. W. STED microscopy with continuous wave beams. *Nature Methods* **4**, 915–918 (2007).
4. Ma, Y., Rui, G., Gu, B. & Cui, Y. Trapping and manipulation of nanoparticles using multifocal optical vortex metalens. *Scientific Reports* **7**, 14611 (2017).
5. Paez-Lopez, R., Ruiz, U., Arrizon, V. & Ramos-Garcia, R. Optical manipulation using optimal annular vortices. *Optics Letters* **41**, 4138 (2016).
6. Wang, J. *et al.* Terabit free-space data transmission employing orbital angular momentum multiplexing. *Nature Photonics* **6**, 488–496 (2012).
7. Willner, A. E. *et al.* Optical communications using orbital angular momentum beams. *Advances in Optics and Photonics* (2015) doi:10.1364/aop.7.000066.
8. Forbes, A., Dudley, A. & McLaren, M. Creation and detection of optical modes with spatial light modulators. *Advances in Optics and Photonics* **8**, 200 (2016).
9. Foo, G., Swartzlander, G. A. & Palacios, D. Optical vortex coronagraph. *Optics Letters* **30**, 3308–3310 (2005).
10. Aleksanyan, A., Kravets, N. & Brasselet, E. Multiple-Star System Adaptive Vortex Coronagraphy Using a Liquid Crystal Light Valve. *Physical Review Letters* **118**, 1–5 (2017).
11. Ruane, G. J. *et al.* Lyot-plane phase masks for improved high-contrast imaging with a vortex coronagraph. *Astronomy & Astrophysics* **583**, A81 (2015).
12. Kujawińska, M., Porras-Aguilar, R. & Zaperty, W. LCoS spatial light modulators as active phase elements of full-field measurement systems and sensors. *Metrology and Measurement Systems* **XIX**, 445–458 (2012).
13. Ashkin, A., Dziedzic, J. M., Bjorkholm, J. E. & Chu, S. Observation of a single-beam gradient force optical trap for dielectric particles. *Optics Letters* **11**, 288 (1986).
14. Liang, Y. *et al.* Aberration correction in holographic optical tweezers using a high-order optical vortex. *Applied Optics* **57**, 3618 (2018).
15. Jahr, W., Velicky, P. & Danzl, J. G. Strategies to maximize performance in STimulated Emission Depletion (STED) nanoscopy of biological specimens. *Methods* **174**, 27–41 (2020).
16. Popiołek-Masajada, A., Frączek, E. & Burnecka, E. Subpixel localization of optical vortices using artificial neural networks. *Metrology and Measurement Systems* **28**, 497–508 (2021).
17. Zolnacz, K., Szatkowski, M., Masajada, J. & Urbanczyk, W. Broadband chromatic dispersion measurements in higher-order modes selectively excited in optical fibers using a spatial light modulator. *Optics Express* **29**, 13256 (2021).
18. Lavery, M. P. J. Vortex instability in turbulent free-space propagation. *New Journal of Physics* **20**, 043023 (2018).
19. Mawet, D. *et al.* Characterization of the inner disk around HD 141569 A from Keck/NIRC2 L-band vortex coronagraphy. *The Astronomical Journal* **153**, 44 (2016).
20. Jesacher, A. *et al.* Wavefront correction of spatial light modulators using an optical vortex image. *Optics Express* **15**, 5801 (2007).
21. Liang, Y. *et al.* Aberration correction in holographic optical tweezers using a high-order optical vortex. *Applied Optics* **57**, 3618 (2018).

22. Wang, W., Yokozeki, T., Ishijima, R., Takeda, M. & Hanson, S. G. Optical vortex metrology based on the core structures of phase singularities in Laguerre-Gauss transform of a speckle pattern. *Optics Express* **14**, 10195 (2006).
23. Shkuratova, V. *et al.* Rapid fabrication of spiral phase plate on fused silica by laser-induced microplasma. *Applied Physics B* **126**, 61 (2020).
24. Oemrawsingh, S. S. R. *et al.* Production and characterization of spiral phase plates for optical wavelengths. *Applied Optics* **43**, 688 (2004).
25. Zheng, Q. *et al.* Astigmatism analysis and correction method introduced by an inclined plate in a convergent optical path. *Applied Optics* **60**, 875 (2021).
26. Kotlyar, V. V., Kovalev, A. A. & Porfirev, A. P. Astigmatic transforms of an optical vortex for measurement of its topological charge. *Applied Optics* **56**, 4095 (2017).
27. Perez-Garcia, B., Yepiz, A., Hernandez-Aranda, R. I., Forbes, A. & Swartzlander, G. A. Digital generation of partially coherent vortex beams. *Optics Letters* **41**, 3471 (2016).
28. Chen, Y., Wang, F., Zhao, C. & Cai, Y. Experimental demonstration of a Laguerre-Gaussian correlated Schell-model vortex beam. *Optics Express* **22**, 5826 (2014).
29. Augustyniak, I., Popiołłek-Masajada, A., Masajada, J. & Drobczyński, S. New scanning technique for the optical vortex microscope. *Applied Optics* **51**, C117 (2012).
30. Szatkowski, M., Popiołek Masajada, A. & Masajada, J. Optical vortex trajectory as a merit function for spatial light modulator correction. *Optics and Lasers in Engineering* **118**, 1–6 (2019).
31. Płocinniczak, Ł., Popiołek-Masajada, A., Masajada, J. & Szatkowski, M. Analytical model of the optical vortex microscope. *Applied Optics* **55**, B20 (2016).
32. Seghilani, M. S., Myara, M., Sellahi, M., Legratiet, L. & Sagnes, I. Vortex Laser based on III-V semiconductor metasurface : direct generation of coherent Laguerre- Gauss modes carrying controlled orbital angular momentum. *Scientific Reports* **6**, 1–12 (2016).
33. Ang, M. E. N. G. W. *et al.* Laguerre-Gaussian beam generation via enhanced intracavity spherical aberration. *Optics Express* **29**, 27783–27790 (2021).
34. Allone, G. I. V *et al.* Birth and evolution of an optical vortex. *Optics Express* **24**, 222–225 (2016).
35. Vallone, G. *et al.* Birth and evolution of an optical vortex. *Optics Express* **24**, 16390 (2016).
36. Szatkowski, M., Norton, B. & Porras-Aguilar, R. Optical vortex quality evaluation. https://github.com/corlic29/vortex_quality_evaluation (2021).